A Light Contamination Ranking Index-based Method for Automating VIIRS Day/Night Band Stray Light Correction

Xi Shao[a], Tung-Chang Liu[a], Sirish Uprety[a], Wenhui Wang[b], Bin Zhang[b], Changyong Cao[c]
[a] Department of Astronomy and Physics, University of Maryland, College Park, MD, USA
[b]Earth Resource Technology, Inc., Laurel, MD, USA,
[c]NOAA/NESDIS/STAR, College Park, MD, USA

ABSTRACT

The Day/Night Band (DNB) of the Visible Infrared Imaging Radiometer Suite (VIIRS) onboard SNPP represents a major advancement in night time imaging capabilities. The DNB senses radiance spanning 7 orders of magnitude in one panchromatic (0.5-0.9 μm) reflective solar band and provides imagery of clouds and other Earth features over illumination levels ranging from full sunlight to quarter moon. When the satellite passes through the day/-night terminator, the DNB sensor is affected by stray light due to solar illumination on the instrument. Current operational stray light correction for Suomi-NPP VIIRS DNB is based on monthly stray light correction Look-up-Table (LUT) which is separated into LUTs for northern and southern hemisphere. Granules with stray light around new Moon are first visually inspected for minimum light contamination such as artificial light, aurora or other light sources and then are selected for stray light correction LUT generation. This paper developed a light contamination ranking index (LCRI)-based algorithm to automate DNB granule selection and stray light correction LUT generation. This method provides means to evaluate the light contamination quantitatively. In this method, an evaluation region is defined across multiple granules in one orbit for northern and southern hemisphere, respectively. The pixel radiance in the prescribed evaluation region is quantitatively scored with Light Contamination Index (LCI), and percentage of pixels with radiance ratio value above the threshold is evaluated. Imagery quality score can be assessed as percentage of bad pixels in the region of interest. The LCI of DNB images are ranked and images with LCI below certain threshold are selected to ensure containing minimum light contamination. This paper demonstrated the effectiveness of LCRI-method in constructing stray light correction LUT and removing stray light from DNB images.

Keywords: S-NPP/VIIRS DNB, DNB calibration, Stray light correction

1. INTRODUCTION

The Suomi National Polar-orbiting Partnership (SNPP) satellite was successfully launched in October 2011 [1-3]. The Day Night Band (DNB) of the Visible Infrared Imaging Radiometer Suite (VIIRS) onboard the SNPP satellite provides imagery of clouds and other Earth features over illumination levels ranging from full sunlight to quarter moon. The DNB sensor utilizes a backside-illuminated charge coupled device (CCD) focal plane array (FPA) for sensing of radiances spanning 7 orders of magnitude in one panchromatic (0.5-0.9 μm) reflective solar band (RSB). In order to cover this extremely broad measurement range, the DNB employs four imaging arrays that comprise three gain stages. The spatial resolution of the DNB is approximately 750m across the entire swath. This is achieved by performing on-chip aggregation of the CCD detector elements to form pixels, which results in 32 aggregation zones through each half of the instrument swath on either side of nadir. The aggregation zones near the end of scan (EOS) have fewer pixels than the zones near nadir, as the footprint of a single CCD detector element on the ground is much larger at EOS. The basic parameters for DNB specifications can be found in Table 1.

Generation of the DNB sensor data record (SDR) product requires accurate knowledge of the dark offsets and gain coefficients for each DNB stage. These are measured on-orbit and stored in lookup tables (LUT) that are used during ground processing. These tables have values for each detector and gain stage. The Low Gain Stage (LGS) gain values are determined by solar diffuser data (aka the onboard calibration). The Medium Gain Stage (MGS) and High Gain Stage (HGS) cannot be calibrated directly using solar diffuser data because these gain stages saturate at solar diffuser illumination levels. Since the three gain stages together cover the entire required radiance range of DNB with sufficient

Earth Observing Systems XXIII, edited by James J. Butler, Xiaoxiong (Jack) Xiong, Xingfa Gu, Proc. of SPIE Vol. 10764, 107641I · © 2018 SPIE · CCC code: 0277-786X/18/$18 · doi: 10.1117/12.2322999

overlap, the MGS and HGS values are determined by multiplying the LGS gains by the MGS/LGS and HGS/LGS gain ratios, respectively. Monitoring and validation of SNPP DNB radiometric accuracy and stability has been routinely performed [4-9]. Long term DNB data were widely used in social-economic studies [10-11] and other applications.

Spectral Band:	0.5 – 0.9μm
Relative radiometric gains	119000: 477: 1 (HGS: MGS: LGS).
Dynamic Range:	L_{max}/L_{min} = 6700000
Number of Bits in A/D:	14 bits (16,384 levels) for HGS; 13 bits (8,192 levels) for MGS and LGS
Spatial Resolution:	750 m
Aggregation:	32 aggregation zones
Time Delay Integration (TDI):	1, 3, and 250 pixels for LGS, MGS, and HGS, respectively
Number of Samples per Scan:	4064
Calibration	Solar diffuser is used to calibrate LGS. MGS and HGS are calibrated with gain ratio derived from data collected along solar terminator region.

Table 1. DNB Design Specifications

The DNB sensor is affected by terminator stray light which is due to solar illumination on the instrument after the satellite passes through the day-night terminator projected on Earth's surface. The stray light is more significant during solstice and most noticeable when the solar zenith angle at the spacecraft falls between 95 degrees to 118.4 degrees. Stray light in the VIIRS DNB imagery is seen on the night side of the terminator that causes a positive offset in radiance when the satellite moves from day to night over the northern hemisphere. Over the southern hemisphere, it starts at the penumbra and becomes insignificant as the spacecraft heads into the day side of the orbit. Northern hemisphere DNB stray light is due to direct sunlight illumination onto Earth view port; Southern hemisphere DNB stray light is due to illumination of Earth view and solar diffuser ports (Figure 1). Stray light depends on the relative orientation of the DNB sensor and the incident sunlight, *i.e.* solar zenith angle, solar azimuthal angle, frame number along scan direction, detector number along track direction, and northern or southern hemisphere.

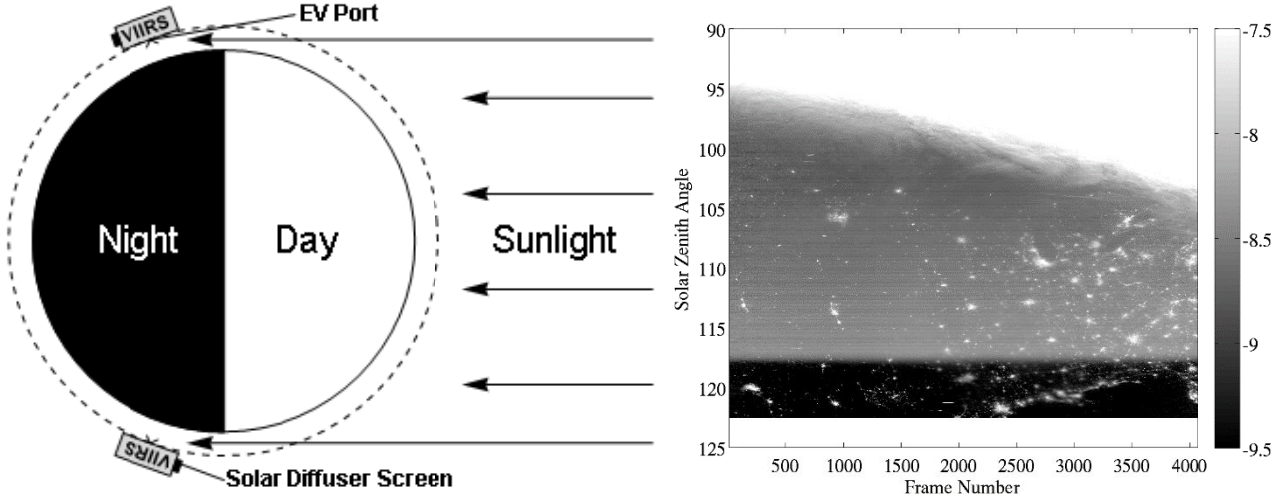

Figure 1: Left: Paths of sunlight illumination onto VIIRS as sources of stray light for DNB in northern and southern hemisphere. Right: Typical northern hemisphere DNB image with stray light contamination. The color scale is rendered in Log(Radiance).

To minimize the stray light effect, stray light LUTs are generated monthly to remove the offset for pixels that are affected. Each LUT is generated by using radiance data with stray light close to the time of a new moon phase that are

not contaminated by aurora or lights related to human activities. In the past, all of the stray light images were visually inspected and were selected for LUT generation based on the criteria such as free from night time lights, free from aurora contamination and free from major clouds. The stray light LUT is indexed according to Hemisphere, Solar Zenith Angle (SZA) (from 95 degrees to 118.4 degrees), Scan Angle, Detector, and half-angle-mirror (HAM) side. This paper developed a light contamination ranking index (LCRI)-based algorithm to automate DNB granule selection (no aurora, artificial light) and stray light correction LUT generation. This method provides means to evaluate the light contamination quantitatively. The LCRI-method was applied to process SNPP DNB data to demonstrate its effectiveness in constructing stray light correction LUT and removing stray light from DNB images.

2. METHODOLOGY

2.1 General Procedure of DNB Stray Light Correction

The general steps involved in DNB stray light correction LUT generation are outlined as following.

1. Data collection: Three days of data impacted by stray light are collected around the new moon (3 days centered on the new moon day). The solar zenith angles are used to determine if a granule is in the stray light region. These granules are sorted by hemisphere. There are typically ~252 impacted granules over each hemisphere during three days.
2. Data selection: Once the data impacted by stray light are collected for all three days, the DNB radiance images are inspected. These regions with stray light typically span ~6 granules on the night side of the terminator in both Northern and Southern hemispheres. The granules within the same orbit are grouped and assembled into images over northern and southern hemisphere, respectively. Granules with cloud or light contamination from light sources such as aurorae or due to human activities need to be discarded to ensure minimum light contamination.
3. Generation and validation of stray light correction LUT
    a. The selected granules form a database. Matlab-based software was used to process the selected granules and generate stray light correction LUT. The stray light LUT is indexed according to Hemisphere, SZA, Scan Angle, Detector, and HAM side. The area contaminated by stray light is separated into one zone and penumbra region in the northern hemisphere and into two zones and penumbra region in the southern hemisphere. An illumination map with man-made lights was used to filter out pixels over known fixed light regions. Staged data from different zones was filtered and fitted with polynomials as function of spacecraft solar zenith angle in 32 bins along the scan direction. The stray light in radiance unit was tabulated as function of discrete solar zenith angle, frame number, detector, HAM side, and hemisphere, to form a matrix and are saved into a binary LUT.
    b. Using the newly generated LUT to process DNB data with stray light and produce DNB image after performing stray light removal. Inspection needs to be performed to assess the effects of stray light removal.
    c. If the effects of stray light removal do not meet expectation, the granules needs to be reselected and the two steps mentioned above will be repeated until the final LUT is confirmed.
4. The stray light correction LUT has been routinely provided to NOAA Interface Data Processing Segment (IDPS) for performing stray light correction on the most recent DNB data. Each LUT has an effectivity window until the next LUT is available.

The quality of DNB stray light correction largely depends on the selection of contamination-free granules. In step 2, visual inspection of assembled granules to select qualified granules was often used which has large uncertainty and is subject to personal judgement bias that can't be quantitatively evaluated. To automate and improve the quality of generating stray light correction LUT, it is critical to quantify the selection process of DNB granules which screens out contamination from aurorae and lights from human activities. Such automation is accomplished by the LCRI-based selection process.

2.2 Light Contamination Ranking Index (LCRI)-based Stray Light Correction Method

The LCRI method uses Light Contamination Index (LCI) to quantitatively score the light contamination in each DNB image consisting of 6 granules assembled over each hemisphere. After grouping and assembling the granules within the same orbit into imagery data over northern and southern hemisphere, respectively. An evaluation region across multiple granules in one orbit with most likely stable signal was chosen to calculate LCI. The LCI-region is defined in terms of solar zenith angle and frame # over each hemisphere, i.e. trapezoid regions with red outline over northern and southern hemisphere as shown in Figure 2. Over the northern hemisphere, the LCI-region is chosen to be away from the day-night terminator region and away from the penumbra region with sharp transition near solar zenith angle =118.4 degree. Over southern hemisphere, since the stray light regions was divided into two zones affected by the stray light from Earth view+ solar diffuser ports and Earth view port, respectively, the LCI-region was chosen to be in the zone affected by stray light leaked from Earth view+ solar diffuser ports.

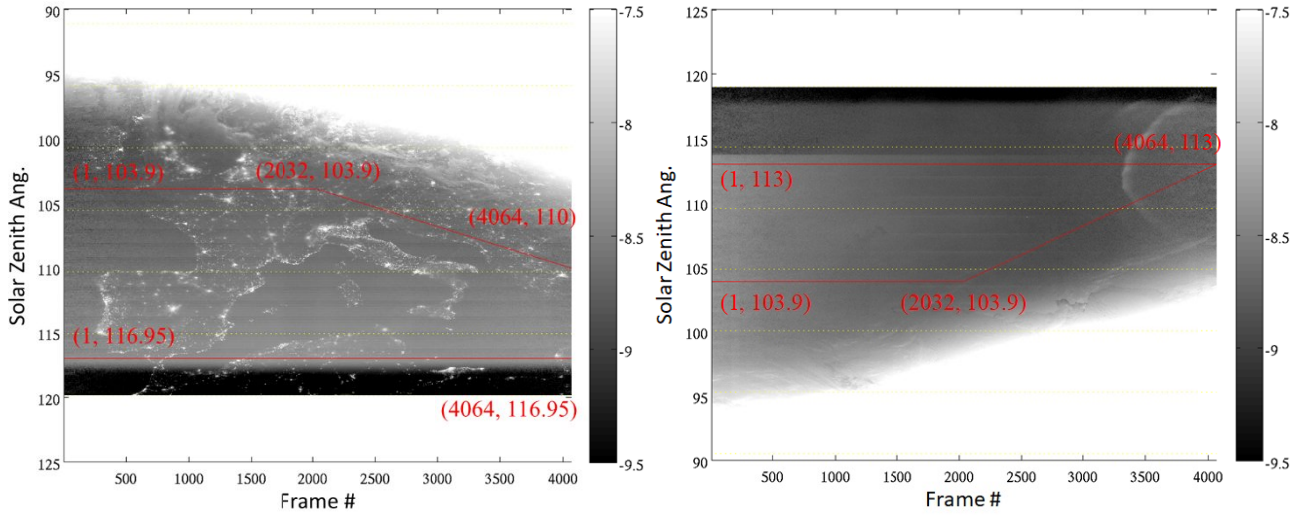

Figure 2: Selected region for calculating LCI over northern (left) and southern (right) hemisphere. The color scale in both panels is rendered in Log(Radiance).

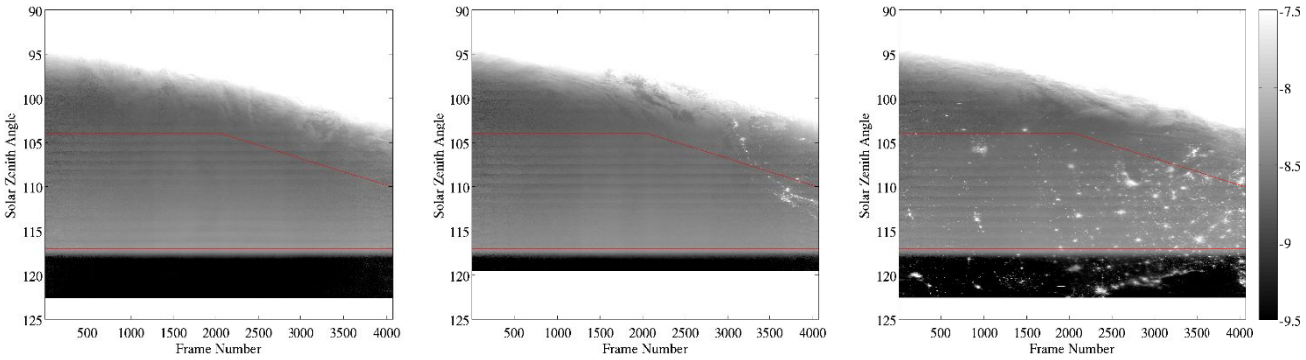

Figure 3: Examples of LCI score of DNB images over northern hemisphere when implementing the LCRI method for stray light correction LUT generation. The color scale in all panels is rendered in Log(radiance).

A seeding LUT generated previously is used to quantitatively score the pixel radiance in the prescribed evaluation region and derive LCI for the image. Each pixel value within the region is normalized by the corresponding stray light value from a seeding or reference stray light correction LUT with the dimension of 2(North/South)×469(Solar Zenith Angle Bins)×4064(Frame along scan direction)×16(Detector)×2(HAM side)]. Using previous stray light LUT assumes that the

spatial and temporal variation of stray light in the LCI-region is insignificant in comparison with the variation due to artificial lights and aurora.

A threshold for the normalized pixel value is set to calculate the percentage of pixels with radiance value above the threshold. Imagery quality score can be assessed as percentage of bad pixels in the region of interest. The less the percentage, *i.e.* LCI score, the better chance for the granule to be clean and selected. Figure 3 and 4 show example of the LCI scores calculated for DNB images over northern and southern hemisphere, respectively, using a threshold = 1.5. Images with aurora and city lights have high LCI score and can be screened out. By ranking the LCI of DNB images and select images with LCI below certain threshold which contains minimum artificial lights, aurora, or other light sources, the selected granules was processed to generate stray light correction LUTs. The LCRI method removes the visual inspection and selection process and made selection criteria more quantitative and objective.

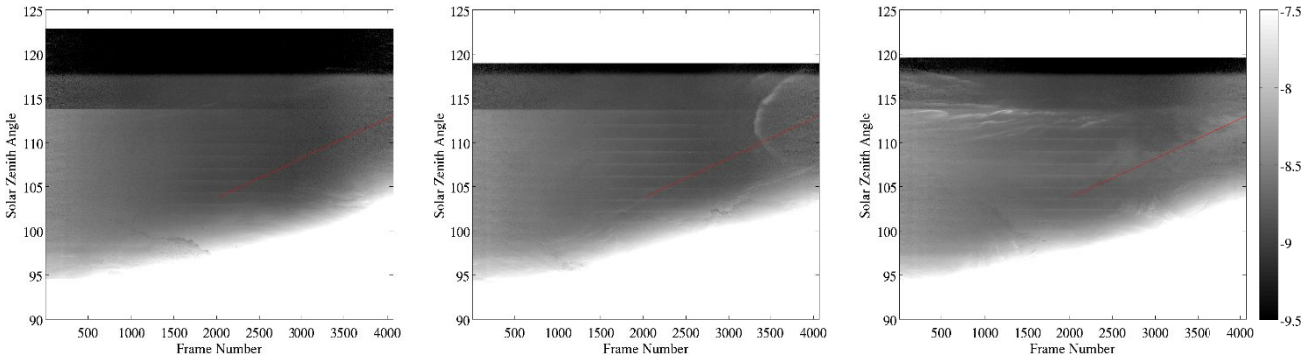

(a) LCI = 0.00129% **(b) LCI = 1.20062%** **(c) LCI = 35.91073%**

Figure 4: LCI evaluation region and examples of using LCI ranking to select DNB images over southern hemisphere for stray light correction LUT generation. The color scale in all panels is rendered in Log(Radiance).

3. APPLICATION OF LCRI METHOD TO SNPP DNB STRAY LIGHT CORRECTION

Using the SNPP DNB stray light correction LUT generation for January, 2017 as an example, Figure 5a and 5b show LCI ranking for stray light-affected SNPP DNB data over northern and southern hemisphere, respectively. In Figure 5, the reference stray light correction LUT used for calculating LCI is the old LUT generated with January, 2015 data. Different thresholds ranging from 100% to 250% w.r.t. the reference LUT have been used and the resulting LCIs are shown in different columns. With the threshold being set as 100%, the LCI is above 90% for assembled granules over both northern and southern hemisphere. The reference stray light correction LUT was generated through statistical regression of staged multiple granules data. There were fluctuations in pixel radiance due to air glow and changes in Sun-Earth-SNPP geometry when the old LUT was generated. Over the northern hemisphere, the orbits were pre-filtered with LCI score < 55% at screening threshold of 125% and then sorted with the LCI score at screening threshold of 200%. Over the southern hemisphere, the LCI score at screening threshold of 150% was sorted. The LCI drops sharply to well below 1% for DNB images over southern hemisphere as tabulated in Figure 5. By targeting the final LCI score being around 1 percent, the pixels with artificial lights and aurora contamination can be effectively screened out. Using such threshold, ten to twelve orbits with lowest LCI were selected for each hemisphere as shown in Figure 5. The granules in these selected orbits have the minimum contamination from artificial lights, aurora or other transient light sources.

Figure 6 shows the color map of stray light correction LUT for northern and southern hemisphere generated with the granules selected by the LCRI method. The LUT has been averaged over detectors and HAM side. The overall stray light magnitude over both hemisphere is less than 5 nW/cm^2-sr. The distribution of stray light is different between northern and southern hemisphere. Over the northern hemisphere, the stray light is stronger near solar zenith angle = 115 degree than those near solar zenith angle = 100 degree. Over the southern hemisphere, the LUT correctly captured the two-zone structure of the stray light which leaked through Earth view port + solar diffuser screen (Zone #1) and through Earth view port alone (Zone #2), respectively. The leaking of stray light through the Earth view port + solar diffuser screen occurred in region with solar zenith angle less than 114 degree and the magnitude was stronger than those leaked through the Earth view port alone. In Zone #1, the stray light is strong in regions with frame number < 500 or > 3500

and weak in-between. Both LUTs show sharp decrease of stray light in penumbra region near the highest solar zenith angle in the LUT to match the stray light-free region beyond solar zenith angle = 118.4 degree.

The stray light correction LUT generated with the LCRI method was applied back and being subtracted from the SNPP DNB SDR data. The performance of the stray light correction was shown in Figure 7 and 8 for northern hemisphere and in Figure 9 for southern hemisphere, respectively. Figure 7 and 9 show the solar zenith angle-dependence of the DNB data (blue circles) collected from the granules selected by the LCRI method for DNB detector # 1 in two sample bins along the scan direction. Together with the DNB sample data, the modeled stray light vs. solar zenith angle from two stray light correction LUTs, e.g. recycled LUT from Jan., 2015 (green line) and LCRI-derived LUT from Jan., 2017 (red line), are also shown. In Figure 7 and 8, the deviation of the recycled stray light LUT of Jan., 2015 from the sample data was remedied by the LCRI-derived stray light correction LUT. This indicates that although the granules were selected using the LCI relative to the old LUT, the LCRI-derived LUT correctly characterized the stray light in the new DNB data.

The performance of the LCRI-method was further evaluated with the DNB images shown in Figure 8 and 9 for northern and southern hemisphere, respectively. DNB images over both hemispheres before and after applying the stray light correction LUT generated with the LCRI method were compared. In Figure 8, the stray light correction effectively revealed fine features of city light distribution and aurora which were masked by the stray light. The 16-detector striping in the stray light-affected region was also removed after applying the stray light correction. In Figure 9, the effectiveness of stray light correction in revealing aurora features of large extent can be clearly seen.

Orbit	100%	125%(<55%)	150%	200%(↑)	250%
27197	99.83509%	52.23801%	15.65023%	0.76456%	0.14572%
27198	99.81424%	42.16034%	11.65379%	0.96585%	0.14914%
27200	99.61813%	47.61063%	11.40403%	1.02356%	0.19027%
27213	99.73178%	44.54524%	12.18013%	1.13855%	0.20448%
27194	98.91696%	38.70000%	11.13379%	1.18973%	0.20376%
27212	99.79597%	42.36001%	11.81723%	1.19019%	0.21992%
27196	99.70914%	38.17293%	11.57141%	1.31592%	0.21659%
27195	99.35864%	36.26000%	11.38419%	1.36308%	0.22180%
27199	99.90479%	50.02332%	14.21774%	1.51115%	0.26909%
27193	99.05205%	39.69182%	14.31863%	1.68582%	0.34216%
27222	99.61991%	50.16743%	16.52002%	1.82150%	0.39327%
27208	99.80924%	54.73887%	23.74903%	1.92589%	0.53344%
27226	99.77236%	54.59309%	16.36746%	2.05888%	0.36664%
27211	99.86730%	52.61923%	20.05469%	2.49657%	0.68430%
27207	99.61301%	50.66442%	22.16961%	5.57694%	2.57329%

(a) Northern Hemisphere

Orbit	100%	125%	150%	200%	250%
27240	95.97223%	13.45196%	0.27270%	0.00015%	0.00007%
27212	95.42742%	10.72613%	0.27685%	0.00026%	0.00002%
27223	91.00297%	11.38222%	0.37582%	0.03054%	0.01999%
27207	97.96880%	25.78208%	0.37671%	0.00015%	0.00000%
27195	93.52489%	14.40753%	0.42024%	0.03466%	0.02324%
27239	98.52997%	27.44095%	0.63829%	0.00040%	0.00002%
27262	98.16931%	24.13012%	0.66874%	0.00049%	0.00000%
27227	97.43540%	22.58410%	0.68588%	0.00099%	0.00004%
27241	95.21378%	27.76922%	0.71427%	0.00024%	0.00007%
27247	97.61180%	28.44577%	0.71531%	0.00020%	0.00000%
27234	97.98796%	25.43526%	0.73000%	0.00011%	0.00002%
27206	98.98569%	35.03654%	0.77226%	0.00031%	0.00000%
27224	95.69230%	21.22935%	0.82205%	0.00686%	0.00540%
27251	98.11461%	21.74537%	0.82817%	0.04316%	0.02881%
27228	96.92572%	23.57153%	0.87659%	0.00035%	0.00002%

(b) Southern Hemisphere

Figure 5: LCI ranking of stray light-affected SNPP DNB data over northern and southern hemisphere around new moon day on Jan. 26, 2017. Green-shaded orbit numbers indicate selected orbits for LUT generation. Multiple threshold ratio w.r.t. reference stray light correction LUT has been used and the corresponding LCI score is shown in different columns.

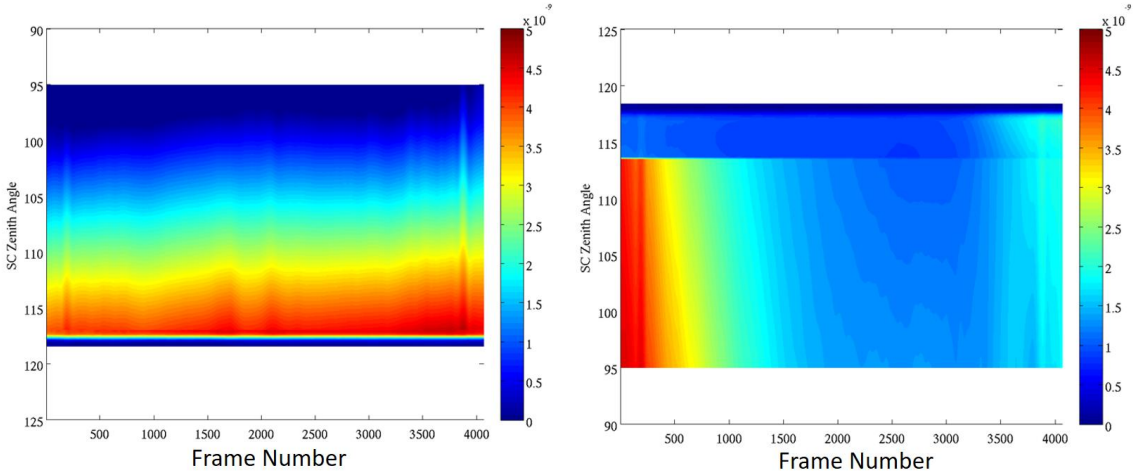

Figure 6: Northern (left) and southern (right) hemisphere DNB stray light correction LUT (averaged over detectors and HAM side) vs. spacecraft solar zenith angle and frame number along the scan direction. The LUTs were genrated using the LCRI method. The color scale in both panels is in linear scale.

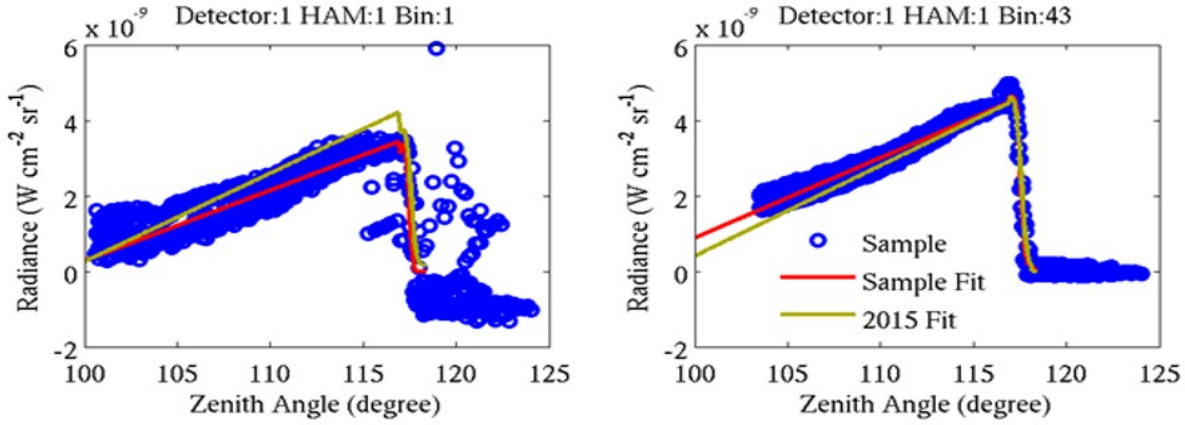

Figure 7: Stray light correction LUTs (recycled operational LUT from Jan., 2015 (green line) and LCRI-derived LUT from Jan., 2017 (red line)) vs. solar zenith angle over northern hemisphere for two selected bins along the scan direction together with sample DNB data (blue circles) collected around January 26, 2017.

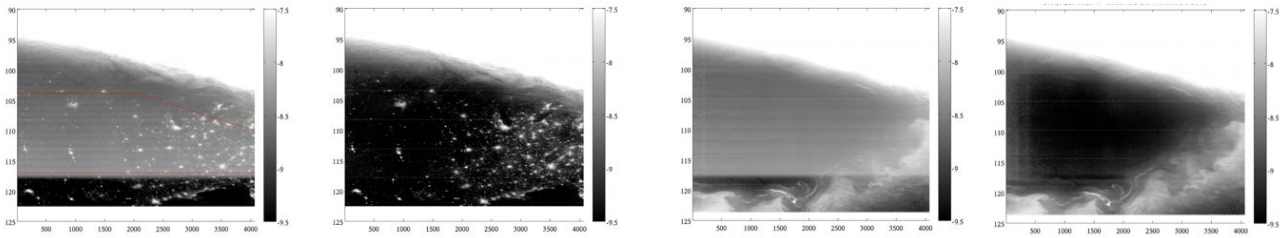

(a) (b) (c) (d)

Figure 8: Example of DNB images over northern hemisphere before (Panel a and c) and (Panel b and d) after applying stray light correction LUT generated with the LCRI method. The color scale in all panels are in Log(Radiance).

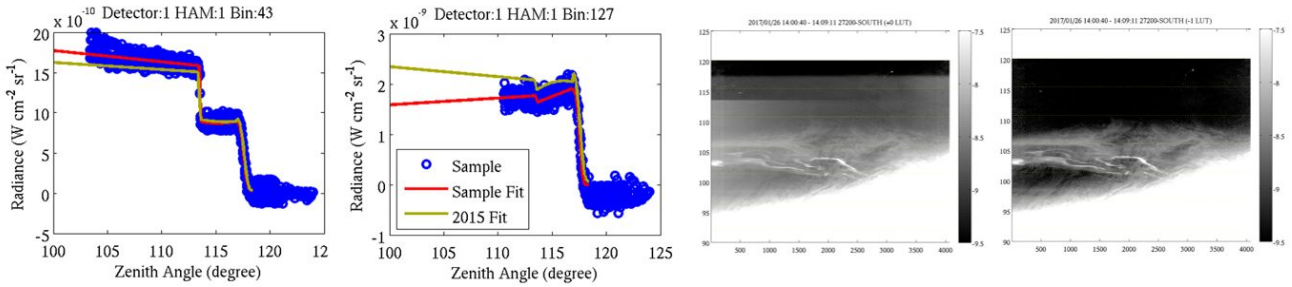

Figure 9: (Two panels on the left) Stray light correction LUTs (recycled operational LUT from Jan., 2015 (green line) and LCRI-derived LUT from Jan., 2017 (red line)) vs. solar zenith angle over southern hemisphere for two selected bins along scan direction together with sample DNB data (blue circles) collected around January 26, 2017. (Two panels on the right) Example of DNB images over southern hemisphere before and after applying stray light correction LUT generated with the LCRI method. The color scale in both panels are in Log(Radiance).

4. SUMMARY

In this paper, a LCRI method has been developed to quantitatively automate good-quality granule (no aurora or artificial light) identification and the DNB stray light correction LUT generation. In this method, evaluation regions over both hemisphere were defined across multiple granules in one orbit with the most likely stable signals. The pixel radiance in the prescribed evaluation region is quantitatively scored with LCI to evaluate the light contamination by artificial light, aurora and other transient light sources. The LCRI method ranked the DNB images with LCI and images with LCI below certain threshold are selected for stray light correction LUT generation. The effectiveness of the LCRI method was demonstrated through the application of the method to construct stray light correction LUT and remove stray light from SNPP DNB data. The LCRI method was also being extended to the NOAA-20 DNB stray light correction LUT generation.

ACKNOWLEDGEMENT

The manuscript contents are solely the opinions of the authors and do not constitute a statement of policy, decision, or position on behalf of NOAA or the U.S. government.

REFERENCES

[1] Cao, C., Xiong, X., Blonski, S., Liu, Q., Uprety, S., Shao, X., Bai, Y., and F. Weng, "Suomi NPP VIIRS Sensor Data Record Verification, Validation and Long Term Performance Monitoring," Journal of Geophysical Research-Atmosphere 118(20), 11664–11678 (2013).

[2] Cao, C., DeLuccia, F., Xiong, X., Wolfe, R., and Weng, F., "Early On-orbit Performance of the Visible Infrared Imaging Radiometer Suite (VIIRS) onboard the Suomi National Polar-orbiting Partnership (S-NPP) Satellite," IEEE Trans. Geosci. and Remote Sens. 52(2), 1142-156 (2014).

[3] Geis, J. C., Florio, J., Moyer, D., Rausch, K. W., and De Luccia, F., "VIIRS day-night band calibration and on-orbit performance," SPIE Proceedings, Earth Observing Systems XVII 8510, (2012).

[4] Liao, L. B., Weiss, S., Mills, S., and Hauss, B., "Suomi NPP VIIRS day-night band on-orbit performance," J. Geophys. Res. Atmos., 118, 12705–12718 (2013).

[5] Shao, X., Cao, C. and Uprety, S., "Vicarious calibration of S-NPP/VIIRS day-night band," SPIE Proceedings Vol. 8866, Earth Observing Systems XVIII 88661, (2013).

[6] Shao, X., Cao, C., Zhang, B., Qiu, S., Elvidge, C., and Von Hendy, M., "Radiometric calibration of DMSP-OLS sensor using VIIRS day/night band," Proceedings of SPIE, Earth Observing Missions and Sensors: Development, Implementation, and Characterization III 9264, (2014).

[7] Qiu, S., Shao, X., Cao, X., and Uprety, S., "Feasibility demonstration for calibrating Suomi-NPP visible infrared imaging radiometer suite day/night band using Dome C and Greenland under moon light," Journal of Applied Remote Sensing, 15219RP (2016).

[8] Qiu, S., Shao, S., Cao, C., Uprety S., and Wang, W., "Assessment of straylight correction performance for the VIIRS Day/Night Band using Dome-C and Greenland under lunar illumination," International Journal of Remote Sensing 38 (21), (2017).
[9] Zeng, X., Shao, X., Qiu, S., Ma, L., Gao, C., and Li, C., "Stability Monitoring of the VIIRS Day/Night Band over Dome C with a Lunar Irradiance Model and BRDF Correction." Remote Sens. 10(189), (2018).
[10] Cao, C., Shao, X., and Uprety, S., "Detecting Light Outages After Severe Storms Using the Suomi-NPP/VIIRS Day Night Band Radiances," IEEE Geoscience and Remote Sensing Letters, 10(6), 1582-1586 (2013).
[11] Jing, X., Shao, X., Cao, C., Fu, X., and Yan, L., "Comparison between the Suomi-NPP Day-Night Band and DMSP-OLS for Correlating Socio-Economic Variables at the Provincial Level in China," Remote Sens. 8(17), (2016).